The Solar Particle Event on 10 September 2017 as observed on-board the International Space Station (ISS)

T. Berger[1], D. Matthiä[1], S. Burmeister[2], R. Rios[4], K. Lee[3], E. Semones[3], D. M. Hassler[5], N. Stoffle[4], C. Zeitlin[4]

[1]German Aerospace Center (DLR), Institute of Aerospace Medicine, Cologne, Germany, [2]Christian Albrechts University (CAU), Kiel, Germany, [3]NASA Johnson Space Center, Houston, TX, USA, [4]Leidos Innovations Corporation, Houston, TX, USA, [5]Southwest Research Institute, Boulder, CO, USA

Corresponding author: Thomas Berger (thomas.berger@dlr.de)

Key Points:

- A Solar Particle Event - also seen as GLE 72 on Earth - was measured in September 2017 inside the International Space Station.
- Data was provided by two detector systems, DOSIS 3D-DOSTEL and ISS-RAD, both in close proximity to each other in the Columbus Laboratory.
- The additional absorbed dose due to the 10 September 2017 Solar Particle Event was in the range of 67.8 to 146.2 µGy in Si.

Abstract

The nominal radiation environment in Low Earth Orbit (LEO), especially for the International Space Station (ISS), is dominated by two sources. The first is galactic cosmic radiation (GCR) which is modulated by the interplanetary and the Earth's magnetic fields and the second is trapped radiation in the form of the Van Allen Belts. The trapped radiation inside the ISS is mostly due to protons of the inner radiation belt. In addition to these sources sporadic Solar Particle Events (SPEs) can produce high doses inside and outside the ISS, depending on the intensity and energy spectrum of the event. Before 2017, the last SPE observed inside the ISS with relevant radiation detectors occurred in May 2012. Even though we are currently approaching the next solar minimum, an SPE was observed in September 2017, which was a) a Ground Level Enhancement (GLE 72); b) measured with various radiation detector systems on-board the ISS and c) observed on the surface of Mars. This paper gives an overview of the 10 September 2017 SPE measured with the DOSIS 3D-DOSTEL and the ISS-RAD (Radiation Assessment Detector) instruments, both located at this time in close proximity to each other in the Columbus Laboratory of the ISS. The additional dose received during the SPE, was 146.2 µGy in Si as measured by ISS-RAD and 67.8 µGy in Si as measured by the DOSIS 3D-DOSTEL instruments. In comparison, the dose measured on the surface of Mars with the MSL-RAD (Mars Science Laboratory) instrument accounted to 418 µGy in Si.

This article has been accepted for publication and undergone full peer review but has not been through the copyediting, typesetting, pagination and proofreading process which may lead to differences between this version and the Version of Record. Please cite this article as doi: 10.1029/2018SW001920

Plain Language Summary

Severe Solar Particle Events can be the source for deterministic radiation effects on humans, commonly summarized under the term "radiation sickness". We examine the evolution of the Solar Particle Event from 10 September 2017 which was the first event since May 2012 seen inside the International Space Station. Radiation dose values are provided by two instruments (DOSIS 3D-DOSTEL and ISS-RAD) positioned in close proximity to each other in the Columbus Laboratory.

1. Introduction

The space radiation environment and its impact on humans has been seen as one of the main problems for long duration human space missions. This is of particular importance for the currently planned exploration missions to the Moon, near Earth asteroids and in the long term future to Mars (Durante & Cucinotta, 2011). The radiation environment in space is composed mostly of galactic cosmic radiation (GCR), which – modulated by the solar activity – provides the overall "background" radiation environment in free space. For long duration missions GCR will be the primary origin of stochastic radiation effects resulting in additional risk of exposure induced cancer (REIC). Another source of radiation are the protons that are accelerated during a Solar Particle Event (SPE). Astronauts on-board the International Space Station (ISS) are protected against high doses from Solar Energetic Protons (SEP) as a result of being shielded by the geomagnetic field for much of its trajectory. This will not be the case for trajectories in free space or on the surface of planetary bodies without a magnetic field or with an insignificant localized magnetic field, such as Mars. For these same missions SPEs will be the primary origin of deterministic radiation effects commonly summarized under the term "radiation sickness" which are based on threshold values. As an example, Table 1 provides the NASA 30 day permissible exposure limits for relevant organs such as 250 mGy-eq for the blood forming organs (BFO) (see also Table 1 in NASA (2014)).

Even though SPEs tend to have lower proton energies in comparison to the GCR proton energy spectrum, some SEPs can have energies at the GeV level, which makes adding additional structural materials and/or dedicated shielding materials for a spacecraft flying in free space (e.g., a storm shelter) a prerequisite for mission planning.

In Low Earth Orbit (LEO), a third source of radiation is the trapped protons and electrons in the Earth's inner and outer radiation belts (Van Allen Belts). This exposure is primarily from the proton contributions while the ISS passes through the South Atlantic Anomaly (SAA); in disturbed geomagnetic conditions even outer belt electrons can be measured inside the lower-shielded parts of ISS. For the time period of September 2017, the contributions of GCR and SAA to the overall dose inside the Columbus Laboratory of the ISS are almost equal (44% GCR, 56% SAA) , resulting in a total daily absorbed dose (in Si) of around 250 µGy as measured with the DOSIS 3D-DOSTEL instruments.

1.1 SPEs on-board MIR and the ISS

Looking at the available SPE measurements in LEO, the majority of data for the 1980´s and 1990´s was collected on-board the Russian MIR Space Station (Petrov et al., 1994; Shurshakov et al., 1999; Badhwar et al., 2002). An especially important time is September and October 1989 where in a disturbed time period we had a total of four Ground Level Enhancements (GLE) from 29 September to 24 October 1989, namely GLE 42 to GLE 45. (see also: http://cosmicrays.oulu.fi/GLE.html). These are the highest SPE doses ever measured in LEO onboard a space station (see: Table 2) resulting in doses of 27 mGy

measured by the R-16 ionization chamber (Shurshakov et al., 1999) for GLE 43 on 19 October 1989.

The newest calculations performed by Kim et al. (2017) for the Event at 19 October 1989 concluded, that "by taking into account a factor of 2 reduction provided by the shadow shield over half of the solid angle on the lunar surface, the exposure estimate from the 19 October 1989 GLE in a lightly shielded vehicle on lunar surface is still over the short-term limit of 150mSv for the whole-body effective dose limit set by NASA for design requirement of rover." (Paragraph from Kim et al. (2017) Section 3.2).

The ISS saw an increase of active radiation detectors applied for various research and operational purposes (Narici et al., 2015), thereby also increasing the data measured and available for comparison (Narici et al., 2017; Rios, 2017). In terms of dose, one of the most significant SPEs for ISS is the so called "Halloween Event" on the 28 and 29 of October 2003 (GLE 65 and GLE 66), which resulted in dose values measured inside the Russian Service module by the DB-8 detector systems (Benghin et al., 2005, 2013) of 0.31 – 1.71 mGy (in Si) for GLE 65 and 0.67 – 6.82 mGy (in Si) for GLE 66. The difference in the dose values measured by the DB-8 units (minimum and maximum dose provided for each respective event) is due to the difference in local shielding – which is especially important for the lower energetic protons of the event. It is also worth mentioning that the "Halloween event" was also measured inside an airplane by an built-in Tissue Equivalent Proportional Counter (TEPC) (Beck et al., 2005) which saw a relative increase in the ambient dose equivalent by 35%.

In the following years, the ALTEA (Anomalous Long Term Effects on Astronauts) instrument (Larosa et al., 2011; Berrilli et al., 2014; Di Fino et al., 2014) provided valuable data for the ion rate composition of SPEs. Also worth mentioning are the two events in March and May 2012, which were measured inside the ISS by ALTEA (Berrilli et al., 2014; Di Fino et al., 2014), by the Liulin-5 instrument as part of the MATROSHKA-R experiment (Semkova et al., 2013, 2014), and outside the ISS by the AMS-02 (Alpha Magnetic Spectrometer) experiment (Bindi et al., 2015, Whitman et al., 2017). These events were also measured outside LEO by the CRaTER (Cosmic Ray Telescope for the Effects of Radiation) (Spence et al., 2010) instrument in lunar orbit (Quinn et al., 2017) (Note: relevant data can be retrieved from: http://crater-web.sr.unh.edu) and MSL-RAD (Mars Science Laboratory-Radiation Assessment Detector) (Hassler et al., 2012) on its way to Mars (Zeitlin et al., 2013). While the increase in dose equivalent due to the event in March 2012 inside the MATROSHKA-R phantom was 0.480 mSv (Semkova et al., 2013), MSL-RAD measured 19.5 mSv in free space (Zeitlin et al., 2013). As mentioned before – no event has been observed inside the ISS since May 2012 – but there have been observations performed outside the ISS with the R3RD2 detector mounted behind very low shielding in the EXPOSE-R2 facility; which showed a maximum dose rate of 87 µGy/min measured on 22 June 2015 (Dachev et al., 2016, 2017). This event was not observed inside the ISS due to the rather low energy of protons from this SPE.

1.2 SPEs observed with DOSTEL type instruments on MIR and the ISS

A short overview of SPE measurements performed with detectors from the DOSTEL (DOSimetry TELescope) family is provided below; note that these are one of the detectors also used in the study of the September 2017 event provided in this paper. The first version of the DOSTEL instrument was used for measurements on-board various Space Shuttle missions (STS-76, STS-81 and STS-84) (Reitz et al., 1998; Beaujean et al., 1999a,b; Singleterry et al., 2001). It was mounted in the Kristall module of the MIR space station from

October 1997 to January 1998 as part of the Active Dosimetry of Charged Particles (ADCP) experiment which was flown as part of the NASA-6 mission to MIR. During this time, it measured the onset of the first GLE of the 23rd Solar Cycle on 6 November 1997 (GLE 55) (Burmeister et al., 2000; Beaujean et al., 2002; Badhwar et al., 2002).

Two additional DOSTEL instruments were used as part of the first European Dosimetry experiment, the DosMap experiment, on-board the US Laboratory (US Lab) of the ISS between March and August 2001 (Reitz et al., 2005). During the DosMap mission, data was collected for two more GLEs, namely GLE 60 (15 April 2001) and GLE 61 (18 April 2001). Table 3 provides a re-evaluation of absorbed daily dose (in Si) measured with the DOSTEL instrument for 10 to 20 April 2001 (Note: Relevant SAA contributions have been removed). The data shown spans five days of quiet time and the onset of the first event (GLE 60) on 15 April as well as the onset of the second event (GLE 61) on 18 April 2001.

The evaluation of these two events is further illustrated in Figure 1 by showing (a) the GOES proton flux data for energies ≥ 100 MeV, (b) the absorbed dose rate in Si measured by the DOSTEL instrument and (c) the cumulative daily absorbed dose in Si for the time of the event. The events from April led to an additional dose (in Si) of 338 µGy including the contributions from the main event on 15 April and the subsequent smaller event 18 April.

1.3 The Sun in September 2017 and the 10 September 2017 SPE (GLE 72)

The most prominent activity of solar cycle 24 occurred in September 2017. The largest solar X-ray flare seen in 12 years, a class X9.3, took place on at 12:24 UTC on 6 September 2017. This eruption was accompanied by a fast expulsion of coronal plasma known as a Coronal Mass Ejection (CME) and an associated interplanetary shock accelerating particles resulting in an enhancement of radiation seen near the Earth known as SPE. This was followed by another large X8.2 flare which took place at 16:06 UTC on Sunday, 10 September 2017 with another very fast CME resulting in a stronger/high-energy SPE. The associated increase in high-energy proton flux from the event on 10 September was promptly seen by the radiation monitoring instruments on a number of spacecraft, including Integral, XMM-Newton, Proba-1, Proba-V, Giove-A, AlphaSat, and Galileo. This type of SPE has been classified as GLE 72 as the particle radiation was sufficiently energetic to reach the Earth's atmosphere and induce secondary neutrons which were detected by neutron monitors at the Earth's surface (Kurt et al., 2018). For further details the reader is referred to: ESA Space Environment X-class Flare and SPE in September 2017.

2. Instrument Description and Simulations

This section will shortly describe the applied radiation detectors for this study, namely the DOSTEL instruments applied in the frame of the DOSIS 3D project on-board the Columbus Laboratory of the ISS (2.1) and the ISS-RAD instrument located in close proximity to the DOSTEL instruments in the aft section of the Columbus Laboratory in September 2017 (2.2). Further on, we will describe the procedures applied for the calculation of the dose increase inside Columbus for the time of the event (2.3).

2.1 The DOSIS 3D-DOSTEL Instruments

The DOSTEL instrument family has established its pedigree with various space missions on-board Space Shuttle flights, the space station MIR, and the ISS (see Section 1.2). In the frame of the DOSIS 3D (Dose Distribution Inside the ISS 3D) project (Berger et al., 2016, 2017), two DOSTEL units are positioned beneath the European Physiology Module

(EPM) Rack for long term dose monitoring on-board the European Columbus Module. For this experiment, the DOSTEL units (-1 and -2) are connected to the DOSTEL Data and Power Unit (DDPU) and mounted inside the so called DOSIS-MAIN-BOX (see: Figure 2).

Inside the DOSIS-MAIN-BOX the DOSTELs are mounted in such a way, that the viewing direction of the telescope of DOSTEL-1 is directed forward (ISS flight direction), whereas DOSTEL-2 is directed perpendicular (Port) to the ISS flight direction. The DDPU provides the two DOSTEL instruments with power, stores the data from the instruments on an SD memory card and provides the interface to the Columbus modules. The DDPU is connected via a former NASA 16V laptop power supply to a 120V Columbus power outlet (SUP outlet). Furthermore the DDPU has a data connection via the EPM LAN interface at the upper right part of the EPM facility. The scientific and housekeeping data are downloaded by the EPM rack via Ethernet connection nominally every four weeks. In order to accomplish this, the EPM rack is activated once a month. The total power consumption of the DOSIS experiment is about 3W @ 16V.

Each DOSTEL houses two passivated implanted planar silicon (PIPS) detectors (D1 and D2) each with a thickness of 315 µm and an active area of 6.93 cm^2 arranged in a telescope geometry mounted at a distance of 15 mm thereby yielding a telescope with an opening angle of 120° and a geometric factor for isotropic irradiation of 824 mm^2 sr. With this detector configuration, the DOSTEL measures count rates and dose rates of radiation hitting a single detector ("dose measurement") with a geometry factor of 43.5 cm^2 sr for isotropic irradiation and coincidental hits in the two detectors with a limited path length in the detectors to derive information about the energy deposition spectra and later on also the linear energy transfer (LET) spectra. The energy deposition ranges (in Si) are 0.069 – 165 MeV for the D1 detector and 0.048 – 66 MeV for the D2 detector.

The hardware was launched with Soyuz 30S on 15 May 2012, installed beneath the EPM rack and started acquiring data on 21 May 2012. Up to now the instruments have measured for over six years at this dedicated position inside Columbus. A more detailed description of the instruments as well as all relevant information about calibration as well as detailed information about data products are given in Berger et al. (2017). We will now only focus on relevant data generated and needed for this comparison paper.

2.1.1 DOSIS 3D-DOSTEL: Data Products

During their operation on orbit, the two DOSTEL units (-1 and -2) independently measure the particle count- and absorbed dose rates in the single DOSTEL detector units (D1 and D2). Count rate and absorbed dose rate information is stored every 100 seconds for GCR-like contributions and a count rate trigger decreases the integration time to 20 seconds for SAA passes. Relevant data for DOSTEL-2 for the nominal single detector count and dose rates in comparison with the ISS-RAD_B sub-detector are provided in Sections 3.1 to 3.3.

The measurement of the energy deposition spectra requires a coincidence in the two detectors (D1 and D2) of each DOSTEL, thereby also limiting the path length of the impinging particles. The integration period for the energy deposition spectra is initially set to 45 minutes. To synchronize data with the orbit of the ISS, the minima in the count rates are used to start a new integration period for the spectra. These minima result from crossing the geomagnetic equator where the magnetic shielding of the Earth's magnetic field has its highest efficiency. The energy deposition spectra are integrated over half orbits from one crossing of the geomagnetic equator to the next. Furthermore, the energy deposition spectra measured during SAA passes are stored separately to take into account the different particle

species inside and outside this region. Energy deposition spectra measured with DOSTEL-2 in coincidence mode are provided in Section 3.3.1.

In addition, it is possible to operate one of the DOSTEL units (DOSTEL-1) in Mode 2 (so-called "Single Event Mode"), where every particle that triggers D1 or D2 leads to the storage of the ADC values for both detectors. Switching between nominal Mode 1 and Mode 2 for DOSTEL-1 is done by using the Mode Switch on the DDPU front panel (see also Figure 2). Mode Switch data from DOSTEL-1 are presented in Section 3.3.2.

2.2 The ISS-RAD Instrument

The ISS-RAD (Radiation Assessment Detector) instrument (see: Figure 3) has some heritage from the MSL-RAD instrument (Hassler et al., 2012) which was the first instrument to measure the radiation environment on the way to Mars (Zeitlin et al., 2013) and has continued to operate on the surface of Mars since August 2012 (Hassler et al., 2014).

ISS-RAD contains two sub-systems, a Charged Particle Detector (CPD) (Zeitlin, 2013; Rios et al., 2013; Rios, 2015) which closely resembles the design and purpose of the MSL-RAD detector head (see: Figure 7 in Hassler et al., 2012) and – specifically made for ISS – the Fast Neutron Detector (FND) (Zeitlin, 2013; Leitgab et al., 2016) which measures neutrons in the 0.5 – 8 MeV energy range. Figure 3 shows a picture of the Rad Detector located beneath the European Biolab Module (BLP) Rack in the Columbus Laboratory in September 2017. The left cylindrical dome contains the CPD while the tower on the right contains the FND.

ISS-RAD was successfully launched to ISS on CRS OA-4 (Orbital Sciences CRS Flight 4) on 6 December 2015 and deployed to the US Lab (Destiny module) on 1 February 2016 at 18:55:10 UTC. Activation and checkout was completed on 1 January 2017, after which time ISS-RAD began working as a survey instrument and has been relocated to different modules within the habitable volume of ISS every three months. ISS-RAD was place in the Columbus Laboratory on 16 August 2017, oriented so that the CPD pointed zenith (see: Figure 3); it stayed in this configuration through 19 September 2017, at which point it was oriented port.

2.2.1 ISS-RAD: Data Products

For the dosimetry and event rate analysis reported here, only the B ($ISS\text{-}RAD_B$) detector in the CPD was used. The B detector is a 300 μm thick silicon p-i-n diode or PIPS (Passivated Implanted Planar Silicon) detector manufactured by Canberra with an active area of 1.92 cm^2, leading to a geometry factor for isotropic irradiation of 12.06 cm^2 sr. The B detector is capable of reading out deposited energies between 0.06 MeV and 500 MeV (in Si). The cyclic flux of protons that stop in the fiducial volume of ISS-RAD are reported in real-time (once a minute). Protons are required to reach the D ($ISS\text{-}RAD_D$) detector; energy is determined using ΔE vs. E. The requirement that protons reach D to be recorded in the flux measurement imposes a minimum energy requirement of 20 MeV.

ISS-RAD produces over 40 different data packet types (ranging from raw energy deposition data to housekeeping) at periodic intervals ranging from seconds to hours. Most of these data packets contain raw science data which can be used to calculate different products like time and charge-resolved energy spectra. The primary science data packet is telemetered over MIL-STD-1553 in real-time/cyclic 1-minute intervals. This data packet includes, but is not limited to, dosimetry for the B, E, and FND detectors and stopping proton flux. Raw energy deposition data and trigger/count rates are available in other packets which are also reported on 1 minute intervals. Proton flux and dosimetry and count rates for the B detector from these packets were further analyzed for all investigations in this work. Bulk

data are downloaded approximately once a week – where ISS-RAD is switched into checkout mode, which temporarily disables detector-readout capabilities. Bulk data download sessions over MIL-STD-1553 take on the order of 3-4 hours to complete, which creates gaps in the data.

2.3 Calculation of the SPE dose inside the ISS

Using the description of the primary proton spectra during the event derived by Matthiä et al. (2018), the dose rates inside the Columbus module have been estimated. For this purpose, a CAD model of the Columbus module on the ISS was used to create a ray-traced shielding distribution (Stoffle et al. 2012; Lee et al., 2016). From the results of the ray tracing, the mass distribution of Columbus and the shielding geometry for a GEANT4 (Agostinelli et al., 2003; Allison et al., 2006, 2016) simulation were derived. The geometry consisted of a shell-like structure of aluminum with a fixed inner radius of 2 m but variable thickness. The mass distribution was used in steps of 0.5 g/cm^2 and the fraction covered by the respective shielding was translated to a corresponding solid angle which was then implemented in the shell geometry for the simulation.

The primary particle spectra during the event are described by Matthiä et al. (2018) as one hour averages. In order to derive the corresponding primary spectra along the ISS orbit, the effective vertical cut-off rigidity (R_C) was calculated for each measurement point of the DOSTEL instrument from the corresponding ISS position. The cut-off rigidity was calculated using the GEANT4/PLANETOCOSMICS tool for the International Geomagnetic Reference Field 12 (Thébault et al., 2015) and the Tsyganenko (1989) model for a K_p index of 2^+, which was the actual K_p index in the 3 hour interval between 06:00 UTC and 09:00 UTC on 11 September 2017, in which the largest dose rates at ISS were measured. To calculate the cut-off rigidity in PLANETOCOSMICS a negatively charged particle of a given rigidity is shot upwards from the location of interest in the magnetosphere. If the particle reaches the boundaries of the simulated geometry, it is flagged as escaping the magnetosphere. On the other hand, if the particle hits the Earth's surface or if the particle has not escaped the magnetosphere after a defined track length (here, 104·Earth radius) it is flagged as non-escaping. This procedure is repeated for number of rigidities and the results are used to calculate the lower cut-off rigidity, the upper cut-off rigidity and the effective cut-off rigidity.

The corresponding effective vertical cut-off rigidity was then converted to a threshold kinetic energy for the primary protons. Additionally, the shielding by the solid angle of Earth was taken into account by multiplying the primary spectra by a factor of 0.67.

The resulting primary proton spectra were then folded with pre-calculated dose response functions for a silicon detector inside the aforementioned spherical geometry. The dose response function depends solely on the proton energy and was calculated with GEANT4 for protons between 10 MeV and 5 GeV isotropically incident on the geometry. To derive the dose response functions, mono-energetic protons were shot on the geometry and the resulting dose in the silicon detector inside the shielding geometry per primary particle fluence was calculated. This results in a dose per fluence value for a given primary energy and repeating the procedure for different energies between the above mentioned thresholds results in the dose response functions.

3. Data Analysis and Results

Section 3 will focus on the analysis of the 10 September 2017 SPE by first giving an overview of the whole September time period (3.1), then focuses on the "disturbed" time of September by looking at daily count and dose rate values from 7 to 16 September (3.2). This

is followed by a short analysis of contributions from outer belt electrons to the dose due to the disturbed magnetic field at the beginning of the event (3.2.1), and finally focusing on the event itself by looking into detail into the timeframe from 10 to 13 September 2017 in Section 3.3.

In the following, we focus on data for which the SAA and immediately-surrounding transition (between GCR and SAA) has been removed. We use a model-based definition, thereby preventing any sensitivity to localized shielding inside or outside the vehicle that utilizes the geomagnetic field intensity (B) and Mc Ilwain L-shell parameter (L) as attributed to ISS's trajectory. We have categorized the SAA using $|B| < 23$ μT and $L < 3$; (Rios, 2017) the remaining environment is thereby categorized as GCR. ISS trajectory has been calculated using the instruments' timestamps and SGP4 (Simplified General Perturbation model); for improved accuracy, we calculate the geomagnetic field using IGRF-12 (International Geomagnetic Reference Field) (Thébault et al., 2015) and L-shell at each point in the trajectory.

3.1 An overview of the instrument data pre-, peri-, and post- the Sep 10 SPE (1 – 22 September)

As previously described in Section 1.3, September 2017 was a busy time on the Sun with a class X9.3 solar flare taking place on at 12:24 UTC on 6 September 2017 accompanied by a Coronal Mass Ejection (CME). This was followed by another largeX8.2 flare which took place at 16:06 UTC on Sunday 10 September 2017 with another very fast CME this time resulting in a stronger high-energy SPE.

To illustrate the disturbed September 2017 time, Figure 4 provides the following information for the time from 1 to 22 of September. The top Panel (a) provides the GOES proton flux for energies $\geq$ 10, 50 and 100 MeV showing the onset of the first event and the final onset of the second (GLE 72) event on 10 September 2017. The following Panel (b) provides the Oulu Neutron Monitor (NM) count rate with the clear Forbush decrease on 8 September and the increase of neutron counts for the 10 September 2017. Interesting to note is that through the whole time after the event, Oulu NM had not recovered from the Forbush decrease. The following Panels (c) and (d) provide the particle rates for the DOSTEL-2 and the ISS-RAD_B sub-detector (Note: max. uncertainties are 4% for DOSTEL-2 and 9% for ISS-RAD) as well as the absorbed dose rates (in Si) (e) and (f) for both instruments. The most prominent feature is of course the increase in particle and dose rate at the 11 September 2017 (partly also on 12 September) – the time the event reached the ISS (or the ISS was in relevant northern and southern high latitude orbits, where the event could be seen). In addition we note high count rates on 9 September and also disturbed count rates at high latitude regions up to 22 September 2017.

3.2 Analysis of dosimetry and event rate data for 7 - 16 September

We now focus on data from the disturbed time period of 7 to 16 September 2017. Figure 5 provides the count rate (a) and absorbed dose rate (b) plots for the DOSTEL-2 and the ISS-RAD_B sub-instrument in relation to the L-shell value for these 9 days.

Immediately visible in Figure 5 are four distinct populations which are clearly separated by L value. The first population is the crossing of the SAA for L values between 1 and 2. The second population is the nominal GCR variation due to the orbit of the ISS for L-shell values 1 – 6 with the nominal minimum at L = 1 and the maximum at L = 6. In addition, a small population is seen (mostly in the particle count rate) for L values between 2.5 and 4

(see: peak in particle count rate in Figure 5a). This population consists of electrons from the outer radiation belt which are seen as bremsstrahlung in the detectors and occur due to the disturbed magnetic field following the Forbush decrease. The fourth populations for $3 \leq L \leq 6$, showing count rates of up to 20 particles/cm^2/sec in ISS-RAD$_B$, are the protons from the SPE.

Count rate versus L and time are further illustrated in Figure 6; please note that SAA-like contributions have been cut out based on the procedure given at the start of Section 3. Here, we clearly see the population of low L-shell value electrons in the days before the 10 September event (mostly on the 9 of September) and the high L-shell value populations of the SPE on the 11 but also still on the 12 September 2017.

Figure 7 provides a comparison of daily count- (a) and dose rates (b) measured from the 7 to the 16 September as a function of L from the two instruments and highlights again the following features: A) 7 September = quiet period; B) 9 September = electrons from the outer belts reach the ISS; C) 11 September = arrival of the protons from the SPE seen for L values ≥ 3; D) 12 September = still protons from the SPE at higher L-shell values plus additional electrons between L values of 3 to 4 and E) 13 to 15 September = mostly additional electrons seen in both instruments. Note: The contribution of these electrons, though prominent in the count rate (a) is almost negligible in the dose rate (b).

3.2.1 DOSIS 3D-DOSTEL-2: Electrons – Bremsstrahlung

To further illustrate the electron/bremsstrahlung contributions, Figure 8 shows three consecutive ISS orbits for the 9 September (07:15 to 09:30 UTC) – the first and the third orbit are southern orbits while the middle orbit is a northern orbit. An interesting feature in the first and third orbit is the double peak structure seen in the count rate of the DOSTEL-2 instrument with an increase in counts by more than a factor of 2 in comparison to the northbound crossing. If one looks at the cumulative dose contributions for the relevant orbits – they are all between 4 to 5 µGy and the peak structure is not reflected at all – or only very small in the dose rate profile as well. This is an indication that the increase in count rate is due to energy depositions in the very low energy range – electrons and/or bremsstrahlung from the outer radiation belts (which is especially more pronounced in southern latitudes).

3.3 Measurements and simulations of the SPE (10 - 13 September)

Data from the 10 to 13 September is further analyzed within this section. Figure 9 provides the GOES proton flux (Panel (a)), the absorbed dose rate in Si for both instruments (Panel (b)), the cumulative absorbed dose (in Si) (Panel (c)), the calculation of the dose values (Panel (d)) and the relevant *Rc* values (Panel (e)) for the time under investigation. Even though the event already began on 16:06 UTC on 10 September, the ISS transited through "safe" orbits until 11 September 04:30 when the first SPE protons where observed by both instruments at high southern latitudes. For the ISS orbit, the major phase of the event started at high southern latitude crossings at 07:30 UTC on 11 September 2017 and it was seen in 9 consecutive southern/northern orbits. The dose measured on the day before the event reached the ISS was (as given in Table 4) 113.6 µGy/day for ISS-RAD$_B$ and 103.7 µGy/day in DOSTEL-2. On 11 September it increased to 244.3 µGy/day for ISS-RAD$_B$ and 163.8 µGy/day in DOSTEL-2. On 12 September we continued to observe an increased dose rate at high latitude regions in both instruments resulting in dose values above the nominal background – 129.1 µGy/day in ISS-RAD$_B$ and 111.4 µGy/day in the DOSTEL-2 instrument. If 10 September is taken as quiet day before the event, the additional dose due to the event was 146.2 µGy in Si as measured by the ISS-RAD$_B$ sub-detector and 67.8 µGy in Si as measured by the DOSTEL-2 instrument.

In comparison to the ISS, MSL-RAD on the surface of Mars observed a dose rate of 0.4 µGy/min at the time of the second "main" peak of the event 07:30 UTC on 11 September 2017, while the onset of the event was already seen on 10 September at around 19:50 UTC. The total dose from the event observed with the MSL-RAD_B sub-detector was 347 µGy in Si (Zeitlin et al., 2018; Ehresmann et al., 2018; Hassler et at., 2018).

Schwadron et al. (2018) concluded that the lens and skin dose on the surface of the Moon would approach the NASA 30 day limits (see: Table 1), however even moderate shielding would reduce the radiation dose below the limits.

We will focus now on the discussion of the calculated dose for the event (see: Section 2.3 for the setup). Figure 9 shows the resulting calculated dose rates (Panel (d)) and the effective vertical cut-off rigidity R_C (Panel (e)). Dose rates in LEO are reduced when comparing to interplanetary space due to: 1) the shielding provided by the Earth blocking about one third of the sky at an altitude of 400 km above ground, and 2) the shielding provided by the magnetosphere which can be expressed by the effective vertical cut-off rigidity R_C which varies along the trajectory. This effectively means that the dose rates in a LEO can reach values of about 2/3 of interplanetary space if the trajectory reaches points of very low cut-off rigidity. Due to the tilt and shift of the magnetic field of Earth, the minimum cut-off rigidities are not reached during each orbit but only along orbits at eastern longitude. Figure 9 (Panel (e)) illustrates the calculated cut-off rigidities along the ISS orbit during the SPE on 10-11 September 2017.

During the initial phase of the event, the ISS was in a longitude range with relatively high cut-off rigidities and reached minimum values at northern and southern latitudes between 2 GV and 5 GV, which correspond to proton kinetic energies between 1.3 GeV and 4.1 GeV. At these energies, however, the SEP intensity was not high enough to increase the dose rates inside Columbus. This is reflected in the measured dose rates following the nominal pattern of GCR intensity variation along the varying cut-off rigidity during the initial hours of the event. This observation is replicated in simulations which do not show any SEP contribution during the first hours of the event. Around 04:00 UTC on 11 September 2017 (12 h to 14 h after the onset of the event), ISS reached longitudes and high latitudes for which the minimum values of the cut-off rigidity were well below 1 GV. Due to the shift and tilt of the magnetic field with respect to the rotation axis of Earth, lower values of the cut-off rigidity are reached at high southern latitudes compared to the northern hemisphere. This means, that the shielding effect at southern latitudes is much weaker and is, for a range of longitudes where cut-off rigidities of about 0.3 GV are reached, almost non-existent. Predictions for the dose rate in silicon at these positions reach 5µGy/min. This is about 25% more than the value measured by ISS-RAD_B and over a factor of 2 more than measurements from DOSTEL.

There are several possible explanations for this discrepancy: 1) the reconstruction of the primary proton spectrum, 2) the modelling of the geomagnetic shielding, 3) the Columbus shielding model and 4) the construction and transport through the simulated Columbus shielding. The overestimation of the dose rates is mostly restricted to the highest peaks, i.e. to those parts of the orbit that have the lowest cut-off rigidity at high southern latitudes. At the northern reversal point, however, the calculated dose rate underestimates the measured dose rates when they are at their maximum. After a few orbits, this behavior is inverted: the calculated dose rates at southern latitudes are lower than at northern latitudes while the

measurements still show the same alternating pattern of high and low dose rates. From this observation, it could be suspected that the discrepancy between the measurement and calculations is, at least partly, due to the non-sufficient preciseness of the magnetic shielding effect. The fact that the total calculated dose in Si over the event was 110 µGy and in good agreement with the measurements could be a sign that the rotation of the magnetic field is not accurately taken into account but averages out between northern and southern latitudes.

3.3.1 DOSIS 3D-DOSTEL-2: Energy Deposition Spectra

For the DOSTEL-2 instrument we additionally looked at the energy deposition spectra of particles. These spectra are measured nominally for all northern and southern orbits (integrated over around 45 minutes and triggered by count rate minima). Since the spectra are GCR/SAA separated and time-resolved, we can generate SAA-free energy deposition spectra.

Figure 10a shows the GCR and GCR-like spectra for the exact 11 orbits of the event seen on 11 September 2017 in comparison to the exact same orbits seen the day before. A "bump" is clearly seen in the GCR spectra on the day of the event. By subtracting these distributions, we are able to generate a "net" SPE energy deposition spectrum (Figure 10b). This clearly "resembles" nominal SAA spectra (see also: Figure 14 in Berger et al. (2017)) – thereby highlighting SPE protons.

3.3.2 DOSIS 3D-DOSTEL-1: Mode Switch Data

As mentioned earlier, while DOSTEL-1 operates in Mode 2, every particle hit in any of the two detectors is recognized and stored in internal memory; this means that ADC values in each detector are stored together. As such, this operative mode is memory and bandwidth intensive. Energy losses in the two detectors due to a single particle can indicate particle species, direction and energy. During the September 2017 SPE, DOSTEL-1 took data in Mode 2 from 11 September 07:59 UTC until 18 September 13:29 UTC. In Figure 11 ALL, one can see the energy deposition in D2 vs D1 during this time period. By using ISS's position and the count rates, the data can be further distinguished between GCR dominated, trapped particle dominated, and SPE particle dominated regions.

Figure 11 GCR, illustrates how the energy deposition spectra appear while in GCR dominated regions. Particles measured on the bisecting line (i.e. they deposited nearly the same amount of energy in each detector) are highly energetic/relativistic particles from galactic cosmic radiation. In addition, some secondary/lower energy particles can be seen as they show up, apart from this line. Lower energetic particles penetrating one of the two detectors lose some of their energy already in this detector and then if they pass the other detector lose even more energy in the second one as explained by the Bethe-Bloch-equation.

Protons, for example, start separating visibly at roughly $\Delta E = 2$ MeV from the bisecting line (Figure 11 SAA). A higher ΔE in D2 than in D1 means the particle first penetrated D1 then D2 and vice versa. The maximum energy a proton could deposit in a 315 µm silicon detector is around 7 MeV; this occurs when a proton stops right at the edge of the detector – this is the "hook shape" shown in Figure 11 SAA. This asymmetry is most clearly visible in the data taken in the region of the SAA and shows that the majority of the low energetic protons reach the detector from the aft side, i.e. first hitting D1 and then D2. Figure 11 SPE, mainly consists of particles arriving during the higher count rates when the SPE occurred in September 2017. Here it can be seen that the lower energetic protons came more symmetrically than during the SAA region measurements while a little asymmetry is still visible due to the higher shielding of ISS in the forward direction. Even though there is still contribution of GCR in the data, a minor branch of low energetic helium can be seen starting

at its separation from the bisectrix at about 10 MeV – penetrating the system from the aft side of Columbus.

3.3.3 ISS-RAD: Proton Flux

Fortunately, direct measurements of protons inside ISS are also possible using the ISS-RAD instrument. One of its real-time data products is stopping proton flux in three energy bins between 20 MeV and 122 MeV in the ISS-RAD_D sub-detector.

Average daily proton flux in the GCR-only environment, with the additional requirement of L > 3, are shown in Figure 12. Data with L > 3 were selected because the SPE was only seen at these high L values (see: Figure 5 and Figure 7). The softening (and general intensification) of the proton spectrum is clearly seen on 11 September, whereas the surrounding days are fairly consistent with the nominal GCR background.

If one uses the 9 and 10 September as quiet times before the event, one can see an increase of lower energetic proton flux (20 to 35 MeV) by a factor of 5.4 on the day of the event. Also, the middle energy proton flux (35 – 72 MeV) increased by a factor of 3.2 and the proton flux in the high energy interval increased by 2.6 over the quiet time. We still see a slight increase above the nominal background on the 12 September – 40% over background for all stopping energy bins.

4. Conclusions

For the first time since May 2012, a SPE which happened on 10 September 2017 (16:06 UTC) was also seen on Earth´s as GLE 72, and has been measured with two silicon-based detector instruments, namely the DOSIS 3D-DOSTEL and the ISS-RAD, on-board the Columbus Module of the ISS. During the September 2017 time frame, these two instruments were located in close proximity to each other beneath two research racks (EPM and BLP) on the aft side of the Columbus Module, providing a perfect time and location for data comparison.

The instruments observed the Forbush decrease and related disturbed magnetic field which was visible in the observation of outer belt electrons from 9 September onwards, mostly seen in the southern hemisphere of the ISS orbits. The event on 10 September was observed on-board the ISS starting at 04:30 UTC on 11 September and resulted in an additional dose of 146 µGy in Si for ISS-RAD_B sub-detector and 68 µGy in Si for the DOSIS 3D-DOSTEL-2 instrument. The difference in the accumulated dose values can be explained by the relevant difference in local shielding, which strongly influences the low energy proton contributions to the dose. GEANT4 calculations of the event lead to a dose value of 110 µGy in Si. In addition, the protons of this SPE have been analyzed by looking at the relevant energy deposition spectra from the DOSIS 3D-DOSTEL instruments and their "preferred" arrival direction (from the aft side of Columbus), due to lower overall shielding, has been verified. Further on the proton flux for three distinct energy channels and the respective evolution of the flux for the event has been measured by the ISS-RAD_D sub-detector instrument.

This was the first SPE observed inside the ISS since May 2012 and in addition it was an event which has been clearly seen by the CRaTER instrument orbiting Moon (Schwadron et al. 2018) and by the MSL-RAD instrument on the surface of Mars where it contributed around 418 µGy in Si of additional dose. With all these instruments, we are now generating a unique data set for comparison of the a) timeline of the event and b) the influences of the event in terms of radiation limits for crews in LEO and for exploration missions.

Acknowledgments

For DOSIS 3D CAU, Kiel, Germany was supported by DLR under Grants 50WB0826, 50WB1026, 50WB1232 and 50WB1533. At DLR, Cologne, DOSIS 3D was supported by the DLR grant FuE-Projekt ‘‘ISS LIFE’’ (Programm RF-FuW, Teilprogramm 475). For DOSIS 3D the authors gratefully acknowledge the support of ESA (Jason Hatton, Rene Demets, Liesbeth De Smet) as well as colleagues from CADMOS (Lourdes Oro Marot, Cécile Thevenot) France, OHB (Matthias Böhme) and DLR-MUSC (Pascaline Kerbeci), Germany.

Analysis of ISS-RAD data was performed under National Aeronautics and Space Administration’s Human Health and Performance Contract No. NNJ15HK11B.

DOSIS-3D-DOSTEL data is available at: http://swe.ssa.esa.int/human-space-flight

The authors would like to thank the Sodankyla Geophysical Observatory and the website teams (http://cosmicrays.oulu.fi) for providing the Oulu neutron monitor data. The authors would like to thank the HIMAC team at NIRS in Japan for providing lots of experiment time for the calibration of the instruments in the frame of various HIMAC Research Projects and especially Hisashi Kitamura, Satoshi Kodaira and Yukio Uchihori.

All of the measurements on-board the ISS would not have been possible without the help and support of our astronauts.

References

Agostinelli, S., Allison, J., Amako, K., Apostolakis, J., Araujo, H., Arce, P. et al. (2003). GEANT4-a simulationdoi: toolkit. *Nuclear Instruments and Methods in Physics Research Section A, 506*(3), 250-303. https://doi.org/10.1016/S0168-9002(03)01368-8

Allison, J., Amako, K., Apostolakis, J., Araujo, H., Arce Dubois, P., Asai, M. et al. (2006). Geant4 developments and applications. *IEEE Transactions on Nuclear Science*, *53*, 270-278. https://doi.org/10.1109/TNS.2006.869826

Allison, J., Amako, K., Apostolakis, J., Arce, P., Asai, M., Aso, T. et al. (2016). Recent developments in GEANT4. *Nuclear Instruments and Methods in Physics Research Section A*, *835*, 186-225. https://doi.org/10.1016/j.nima.2016.06.125

Badhwar, G. D., Atwell, W., Reitz, G., Beaujean, R., Heinrich, W. (2002). Radiation measurements on the Mir Orbital Station. *Radiation Measurements, 35*(5), 393–422. https://doi.org/10.1016/S1350-4487(02)00072-0

Beck, P., Latocha, M., Rollet, S., Stehno, G. (2005). TEPC reference measurements at aircraft altitudes during a solar storm. *Advances in Space Research, 36*, 1627–1633. https://doi.org/10.1016/j.asr.2005.05.035

Benghin, V. V., Petrov, V. M., Kireeva, S. A., Markov, A. V., Volkov, A. N., Aleksandrin, A. P. et al. (2005). Analysis of radiation dose increases caused by solar cosmic ray events observed by the Radiation Monitoring System on the Russian Segment of the International Space Station. *Advances in Space Research, 36*(9), 1749–1752. https://doi.org/10.1016/j.asr.2005.08.008

Benghin V. V., Petrov, V.M., Panasyuk, M.I., Nechaev, O.Yu., Nikolaev, I.V., Volkov, A.N. et al. (2013). *Results of the Radiation Monitoring System Measurements on Service Module of ISS during 2009–2013*. Paper presented at 18th Workshop on Radiation Monitoring for the International Space Station, 3–5 September 2013, Budapest, Hungary. Retrieved from http://www.wrmiss.org/workshops/eighteenth/Benghin.pdf

Beaujean, R., Kopp, J., Reitz, G. (1999a). Active dosimetry on recent space flights. *Radiation Protection Dosimetry*, *85*(1–4), 223-226.

Beaujean, R., Reitz, G., Kopp, J. (1999b). Recent European measurements inside Biorack. *Mutation Research*, *430*(2), 183-189. https://doi.org/10.1016/S0027-5107(99)00129-3

Beaujean, R., Kopp, J., Burmeister, S., Petersen, F., Reitz, G. (2002). Dosimetry inside MIR station using a silicon detector telescope (DOSTEL). *Radiation Measurements*, *35*(5), 433-438. https://doi.org/10.1016/S1350-4487(02)00074-4

Berger, T., Przybyla, B., Matthiä, D., Reitz, G., Burmeister, S., Labrenz J. et al. (2016). DOSIS & DOSIS 3D: Long term dose monitoring onboard the Columbus Laboratory of the International Space Station (ISS). *Journal of Space Weather and Space Climate*, *6*, A39. https://doi.org/10.1051/swsc/2016034

Berger, T., Burmeister, S., Matthiä, D., Przybyla, B., Reitz, G., Bilski. P. et al. (2017). DOSIS & DOSIS 3D: radiation measurements with the DOSTEL instruments onboard the Columbus Laboratory of the ISS in the years 2009–2016. *Journal of Space Weather and Space Climate*, *7*, A8. https://doi.org/10.1051/swsc/2017005

Berrilli, F., Casolino, M., Del Moro, D., Di Fino, L., Larosa, M., Narici, L. et al. (2014). The relativistic solar particle event of May 17th, 2012 observed on board the International Space Station. *Journal of Space Weather and Space Climate*, 4, A16. https://doi.org/10.1051/swsc/2014014

Bindi, V. (2015). *Solar Energetic Particles measures by AMS-02*. Proc. 34th International Cosmic Ray Conference, 30 July – 06 August, 2015, The Hague, The Netherlands. Retrieved from http://www.phys.hawaii.edu/ams02/pubs/SEP_AMS_Bindi_ICRC2015.pdf

Burmeister, S., Beaujean, R., Kopp, J., Reitz, G. (2000). *Data on Radiation Belt and Solar Energetic Particles deduced from Dosimetry in Low Earth Orbits.* Paper presented at 5th Workshop on Radiation Monitoring for the International Space Station, 07–08 September 2000, Louvain-La-Neuve, Belgium. Retrieved from http://www.wrmiss.org/workshops/fifth/burmeister.pdf

Dachev, T. P., Tomov, B. T., Matviichuk, Y. N., Dimitrov, P. G., Bankov, N. G. (2016). High dose rates obtained outside ISS in June 2015 during SEP event, *Life Sciences in Space Research*, *9*, 84–92. https://doi.org/10.1016/j.lssr.2016.03.004

Dachev, T. P., Bankov, N. G., Tomov, B. T., Matviichuk, Y. N., Dimitrov, P. G., Häder, D. P., Horneck, G. (2017). Overview of the ISS radiation environment observed during the ESA EXPOSE-R2 mission in 2014–2016. *Space Weather*, *15*, 1475–1489. https://doi.org/10.1002/2016SW001580

Durante, M., & Cucinotta, F.A. (2011). Physical basis of radiation protection in space travel. *Review of Modern Physics, 83*, 1245–1281. https://doi.org/10.1103/RevModPhys.83.1245

Di Fino, L., Zaconte, V., Stangalini, M., Sparvoli, R., Picozza, P., Piazzesi, R., et al. (2014). Solar particle event detected by ALTEA on board the International Space Station - The March 7th, 2012 X5.4 flare. *Journal of Space Weather and Space Climate, 4*, A19. https://doi.org/10.1051/swsc/2014015

Ehresmann, B., Hassler, D. M., Zeitlin, C., Guo, J., Wimmer-Schweingruber, R. F, Matthiä, D. et al. (2018). Energetic Particle Radiation Environment Observed by RAD on the Surface of Mars during the September 2017 Event. *Geophysical Research Letters*, https://doi.org/10.1029/2018GL077801

Hassler, D. M., Zeitlin, C., Wimmer-Schweingruber, R. F., Bottcher, S., Martin, C., Andrews, J. et al. (2012). The radiation assessment detector (RAD) investigation. *Space Science Reviews*, *170*, 503–558. https://doi.org/10.1007/s11214-012-9913-1

Hassler, D. M., Zeitlin, C., Wimmer-Schweingruber, R. F., Ehresmann, B., Rafkin, S., Eigenbrode, J. L. et al. (2014). Mars' surface radiation environment measured with the Mars Science Laboratory's Curiosity rover. *Science*, *343*, p.1244797. https://doi.org/10.1126/science.1244797

Hassler, D. M., Zeitlin, C., Ehresmann, B., Wimmer-Schweingruber, R.F., Guo, J., Burmeister, S., et al. (2018). Space Weather on the Surface of Mars: Impact of the September 2017 Events. *Space Weather*, (This issue)

Kim, M.-H. Y., Blattnig, S. R., Clowdsley, M. C., Norman, R. B. (2017). Using spectral shape and predictor fluence to evaluate temporal dependence of exposures from solar particle events. *Space Weather*, *15*, 374–391. https://doi/org/10.1002/2016SW001552

Kurt, V., Belov, A., Kudela, K., Yushkov, B. (2018). Some characteristics of GLE on 10 September 2017. *Contributions of the Astronomical Observatory Skalnaté Pleso, 48*, 329-338. https://arxiv.org/pdf/1806.00226.pdf

Larosa, M., Agostini, F., Casolino, M., De Santis, C., Di Fino, L., La Tessa, C. et al. (2011). Ion rates in the International Space Station during the December 2006 Solar Particle Event. *Journal of Physics G: Nuclear and Particle Physics, 38*, 095102. https://doi.org/10.1088/0954-3899/38/9/095102

Lee, K., Semones, E., Nounu, H., Stoffle, N., Barzilla, J., Gaza, R., Rios, R. (2016). *Comparison of RAM dose data with calculated dose using an updated ISS CAD.* Paper presented at 21st Workshop on Radiation Monitoring for the International Space Station, 06-08 September 2016, ESA-ESTEC, Noordwijk, The Netherlands. Retrieved from: http://www.wrmiss.org/workshops/twentyfirst/Lee.pdf

Leitgab, M., Rios, R., Semones, E., Zeitlin, C. (2016). *ISS-RAD Fast Neutron Detector (FND) ACO On-Orbit Neutron Dose Equivalent and Energy Spectrum Analysis Status.* Paper presented at 21st Workshop on Radiation Monitoring for the International Space Station, 06-08 September 2016, ESA-ESTEC, Noordwijk, The Netherlands.
Retrieved from http://www.wrmiss.org/workshops/twentyfirst/Leitgab.pdf

Matthiä, D., Meier, M., Berger, T. (2018). The solar particle event on 10-13 September 2017 – Spectral reconstruction and calculation of the radiation exposure in aviation and space. *Space Weather,* (This issue)

Narici, L., Berger, T., Matthiä, D., Reitz, G. (2015). Radiation Measurements Performed with Active Detectors Relevant for Human Space Exploration. *Frontiers in Oncology, 5,* 273. https://doi.org/10.3389/fonc.2015.00273

Narici, L., Berger, T., Burmeister, S., Di Fino, L., Rizzo, A., Matthiä D., Reitz, G. (2017). Exploiting different active silicon detectors in the International Space Station: ALTEA and DOSTEL galactic cosmic radiation (GCR) measurements. *Journal of Space Weather and Space Climate, 7,* A18. https://doi.org/10.1051/swsc/2017016

NASA (2014). NASA SPACE Flight Human-System Standard Volume 1, Revision A: Crew Health, NASA-STD-3001, Vol 1, Rev A; NASA Technical Standards. Retrieved from: https://www.nasa.gov/hhp/standards

Petrov, M. V., Machmutov, V. S., Panova, N. A., Shurshakov, V. V., Dachev, T. P., Matviichuk, Y. N., Semkova, J. V. (1994). Peculiarities of the solar proton events of October 19, 1989 and March 23, 1991 according to the measurements on board the MIR space station. *Advances in Space Research, 14,* 645–650. https://doi.org/10.1016/0273-1177(94)90520-7

Quinn, P. R., Schwadron, N. A., Townsend, L. W., Wimmer-Schweingruber, R. F., Case, A. W., Spence, H. E. et al. (2017). Modeling the effectiveness of shielding in the earth-moon-mars radiation environment using PREDICCS: five solar events in 2012. *Journal of Space Weather and Space Climate, 7,* A16. https://doi.org/10.1051/swsc/2017014

Reitz, G., Beaujean, R., Heilmann, C., Kopp, J., Leicher, M., Strauch, K. (1998). Results of dosimetric measurements in space missions. *Advances in Space Research, 22*(4), 495-500. https://doi.org/10.1016/S0027-5107(99)00129-3

Reitz, G., Beaujean, R., Benton, E., Burmeister, S., Dachev, T., Deme, S., et al. (2005). Space radiation measurements on-board ISS-The DOSMAP experiment. *Radiation Protection Dosimetry, 116*(1–4), 374–379. https://doi.org/10.1093/rpd/nci262

Rios, R., Beard, K.B., Semones, E. (2013). *Status of the International Space Station Radiation Assessment Detector*. Paper presented at 18th Workshop on Radiation Monitoring for the International Space Station, 03-05 September 2013, Budapest, Hungary. Retrieved from http://www.wrmiss.org/workshops/eighteenth/Rios.pdf

Rios, R. (2015). *ISS-RAD: Charged Particle Detector*. Paper presented at 20th Workshop on Radiation Monitoring for the International Space Station, 08-10 September 2015, Cologne, Germany. Retrieved from http://www.wrmiss.org/workshops/twentieth/Rios.pdf

Rios, R. (2017). *Comparison of Silicon-Based Detectors.* Paper presented at 22nd Workshop on Radiation Monitoring for the International Space Station, 05-07 September 2017, Turino, Italy. Retrieved from: http://www.wrmiss.org/workshops/twentysecond/Rios.pdf

Schwadron, N. A., Rahmanifard, F.,Wilson, J., Jordan, A. P., Spence, H. E., Joyce, C. J. et al. (2018). Update on the worsening particle radiation environment observed by CRaTER and implications for future human deep-space exploration. *Space Weather*, *16*, 289–303. https://doi.org/10.1002/2017SW001803

Semkova, J., Dachev, T., Koleva, R., Maltchev, S., Bankov, N., Benghin, V. et al. (2013). Radiation environment on the international space station during the solar particle events in March 2012. *Astrol. Outreach*, *1*, 102. https://doi.org10.4172/2332-2519.1000102

Semkova, J., Dachev, T., Koleva, R., Bankov, N., Maltchev, S., Benghin, V. et al. (2014). Observation of radiation environment in the International Space Station in 2012–March 2013 by Liulin-5 particle telescope. *Journal of Space Weather and Space Climate 4*, A32. https://doi.org/10.1051/swsc/2014029

Shurshakov, V. A., Petrov, V. M., Ivanov, Y. V., Bondarenko, V. A., Tzetlin, V. V., Makhmutov, V. S. et al. (1999). Solar particle events observed on MIR station. *Radiation Measurements*, *30*(3), 317–325. https://doi.org/10.1016/S1350-4487(99)00058-X

Singleterry, R. C., Badavi, F. F., Shinn, J. L., Cucinotta, F. A., Badhwar, G. D., Clowdsley, M. S. et al. (2001). Estimation of neutron and other radiation exposure components in low earth orbit. *Radiation Measurements*, *33*(3), 355-360. https://doi.org/10.1016/S1350-4487(01)00049-X

Spence, H. E., Case, A. W., Golightly, M. J., Heine, T., Larsen, B. A., Blake, J. B. et al. (2010). CRaTER: the cosmic ray telescope for the effects of radiation experiment on the lunar reconnaissance orbiter mission. *Space Science Reviews*, *150*, 243–284. https://doi.org/10.1007/s11214-009-9584-8

Stoffle, N., Welton, A., Barzilla, J., Gaza, R., Lee, K., Zapp, N. (2012) *CAD Shielding Analysis of the International Space Station.* Paper presented at 17th Workshop on Radiation Monitoring for the International Space Station, 04–06 September 2012, Austin, Texas, USA. Retrieved from: http://www.wrmiss.org/workshops/seventeenth/Stoffle.pdf

Thébault, E., Finlay, C. C., Beggan, C. D., Alken, P., Aubert, J., Barrois, O. et al. (2015). International geomagnetic reference field: the 12th generation. *Earth, Planets and Space*, *67*(1), 79. https://doi.org/10.1186/s40623-015-0228-9

Tsyganenko, N. (1989). A magnetospheric magnetic field model with a warped tail current sheet. *Planetary and Space Science*, *37*(1), 5-20. https://doi.org/10.1016/0032-0633(89)90066-4

Whitman, K., Bindi, V., Consolandi, C., Corti, C., Yamashiro, B. (2017). Implications of improved measurements of the highest energy SPEs by AMS and PAMELA. *Advances in Space Research, 60*, 768-780. https://doi.org/10.1016/j.asr.2017.02.042

Zeitlin, C., Hassler, D. M., Cucinotta, F. A., Ehresmann, B., Wimmer-Schweingruber, R. F., Brinza, D.E. et al. (2013). Measurements of energetic particle radiation in transit to mars on the mars science laboratory. *Science, 340*, 1080–1084. https://doi.org/10.1126/science.1235989

Zeitlin, C. (2013). *ISS-RAD Calibration Campaign*. Paper presented at 18th Workshop on Radiation Monitoring for the International Space Station, 03-05 September, 2013, Budapest, Hungary. Retrieved from http://www.wrmiss.org/workshops/eighteenth/Zeitlin_ISS-RAD.pdf

Zeitlin, C., Hassler, D. M., Guo, J., Ehresmann, B., Wimmer-Schweingruber, R. F., Rafkin, S. C. et al. (2018). Investigation of the Radiation Hazard Observed by RAD on the Surface of Mars during the Sept 2017 Solar Particle Event. *Geophysical Research Letters*, https://doi.org/10.1029/2018GL077760

Table 1

NASA 30-day limits (NASA 2014)

Organ	30-Day limit (mGy-eq)
Lens	1000
Skin	1500
BFO	250
Circulatory System	250

NOTE: Data is taken as excerpt from Table 1 in NASA (2014)

Table 2

The dose values for relevant SPEs onboard MIR measured with R-16

Date	GLE	D (R-16) (mGy)
29.09.1989	42	4.9
19.10.1989	43	27.0
23.10.1989	44	2.9
25.10.1989	45	1.4

NOTE: Data is taken as excerpt from Table 2 in Shurshakov et al. (1999)

Table 4

Daily and SPE dose (no SAA) for ISS-RAD$_B$ and DOSTEL-2 instrument

Date	ISS-RAD$_B$	DOSTEL-2
	D (μGy) in Si	
10.09.2017	113.6	103.7
11.09.2017	244.3	163.8
12.09.2017	129.1	111.4
SPE dose	146.2	67.8

Table 3

Daily dose (no SAA) for the DOSTEL instrument

Date (dd.mm) in 2001	D (μGy/day) in Si
10.04	63.2
11.04	62.6
12.04	55.3
13.04	55.6
14.04	56.9
15.04	249.0
16.04	127.4
17.04	69.5
18.04	117.3
19.04	69.7
20.04	60.0

Figure 1. The April 2001 SPEs (GLE 60 and GLE 61) from 14 to 20 of April 2001; (a) GOES data for protons ≥ 100 MeV; (b) DOSTEL absorbed dose rate in Si (µGy/min); (c) DOSTEL cumulative absorbed dose in Si (µGy). Note: contributions from SAA crossings have been removed from (b) and (c)

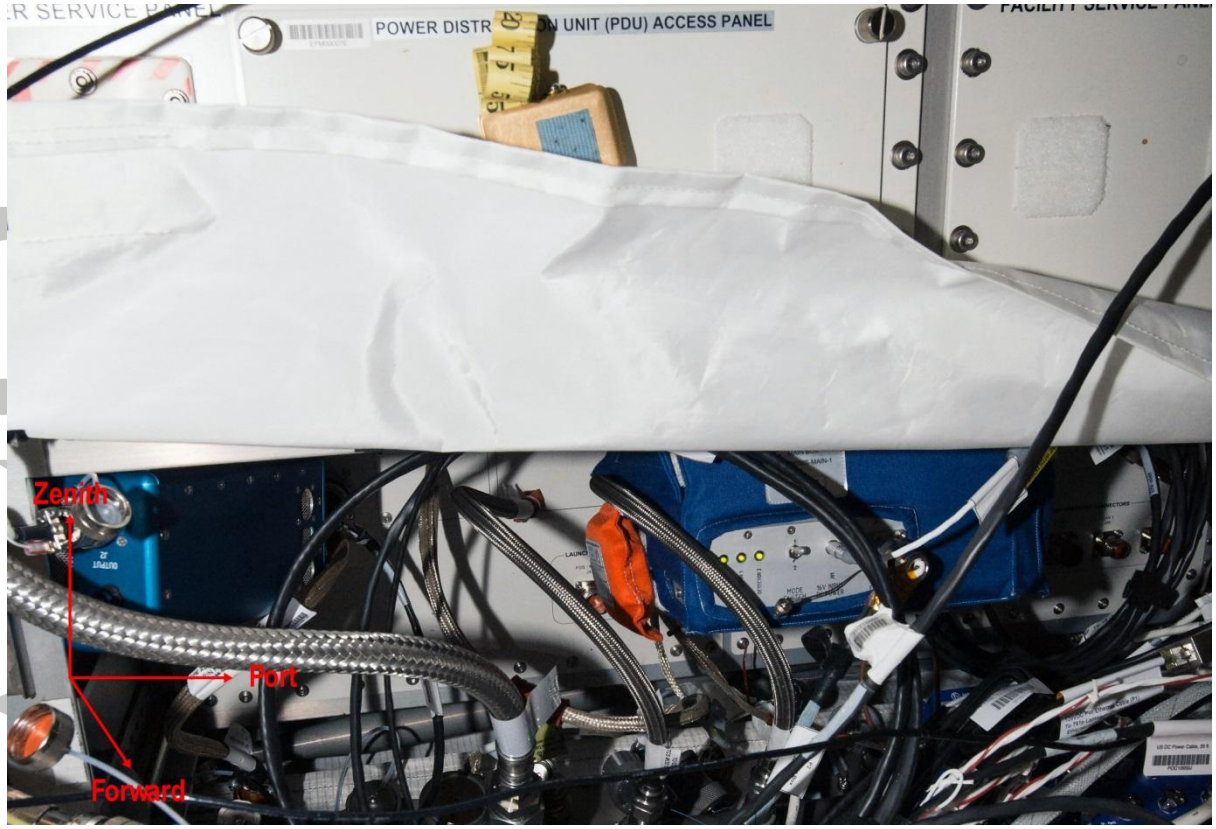

Figure 2. The DOSIS-MAIN-BOX (blue Nomex pouch) with the two DOSTEL instruments located beneath the European Physiology Module (EPM) Rack in Columbus. Note: The small orange Nomex pouch located at the left side of the DOSIS-MAIN-BOX is one of the passive radiation detector (PDP) packages distributed at eleven locations within Columbus in the frame of the DOSIS 3D project (Berger et al., 2016) © ESA, DLR.

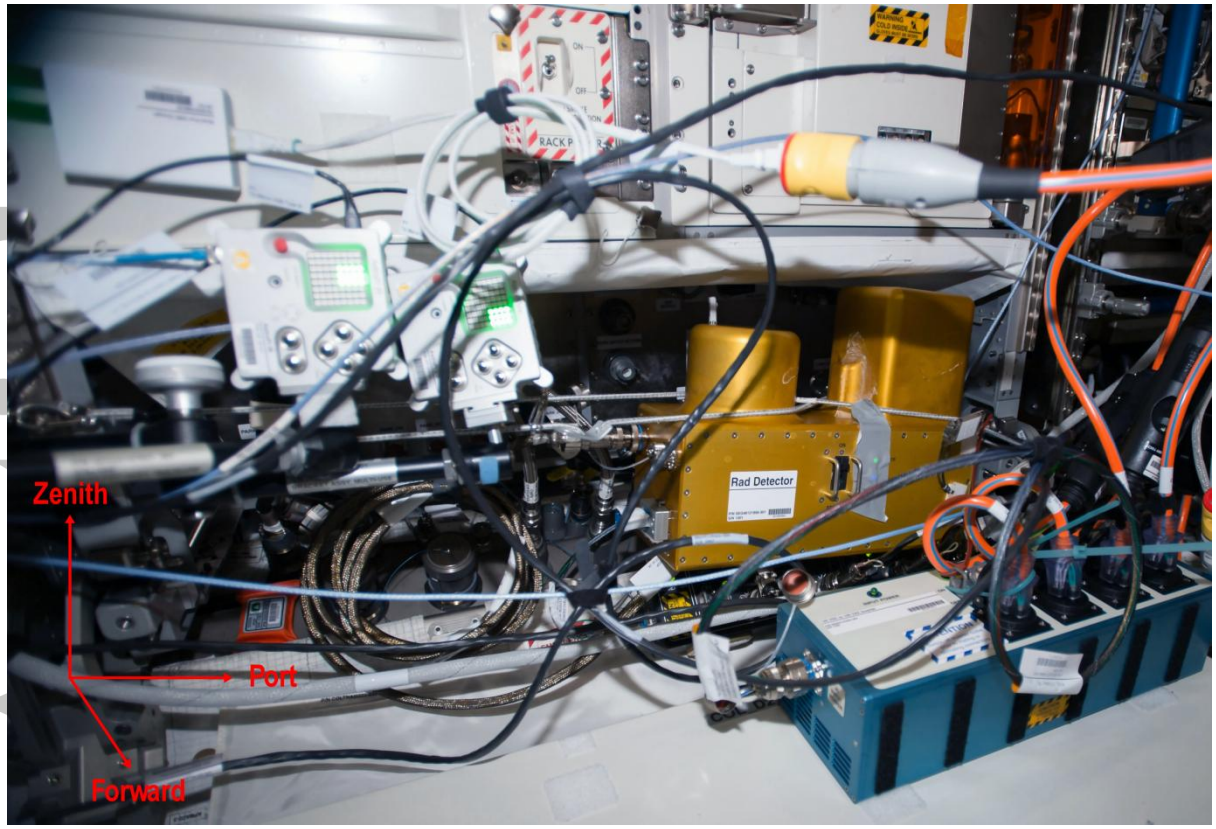

Figure 3. The ISS-RAD instrument (OpNom: Rad Detector) located beneath the European Biolab Module (BLP) Rack in Columbus. The left dome is the Charged Particle Telescope (CPD) with a heritage design based on the MSL-RAD instrument while the right tower contains the Fast Neutron Detector (FND). Note: The small orange Nomex pouch in the lower left part of the picture is one of the passive radiation detector (PDP) packages distributed at eleven locations within Columbus in the frame of the DOSIS 3D project (Berger et al., 2016) © NASA.

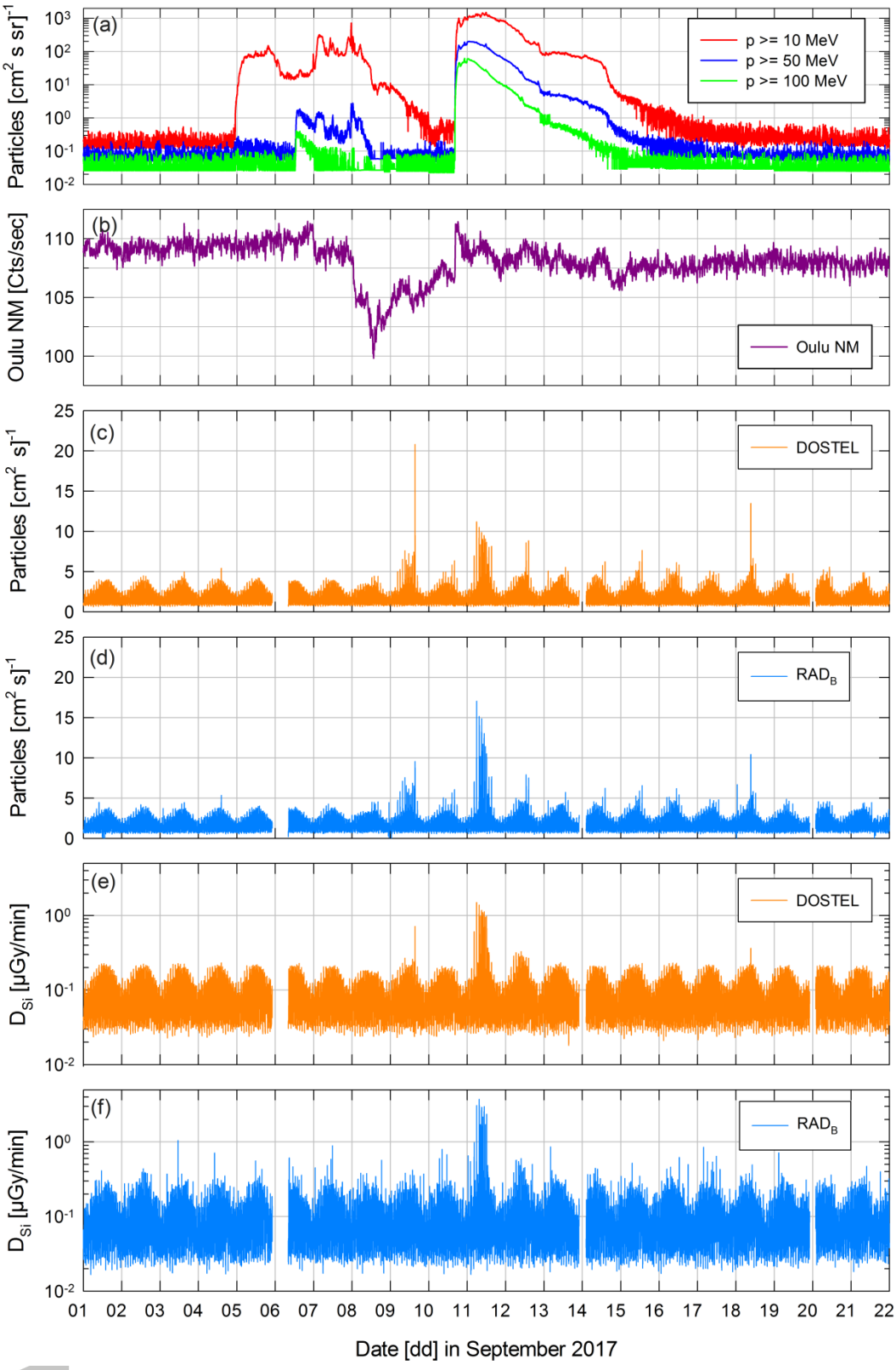

Figure 4. (a) GOES proton flux for p ≥ 10 MeV, p ≥ 50 MeV and p ≥ 100 MeV; (b) Oulu NM count rate; (c) count rate - DOSTEL-2 instrument; (d) count rate - ISS-RAD$_B$ sub-detector; (e) absorbed dose rate in Si - DOSTEL-2 instrument; (f) absorbed dose rate in Si - ISS-RAD$_B$ sub-detector. NOTE: SAA contributions to count and dose rate have been removed based on the procedure given in Section 3.

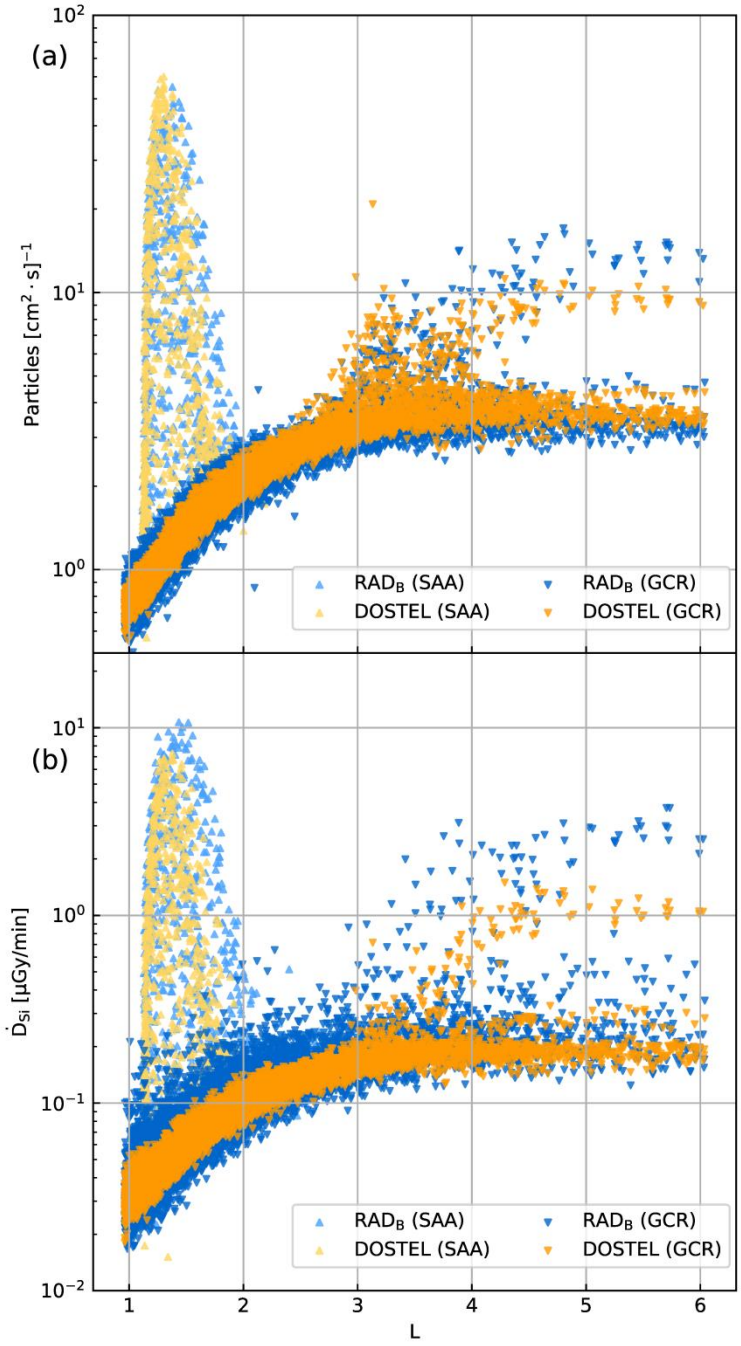

Figure 5. (a) Count rates and (b) absorbed dose rates in Si for the DOSTEL-2 instrument and ISS-RAD_B sub-detector for 07 – 16 September as a function of L.

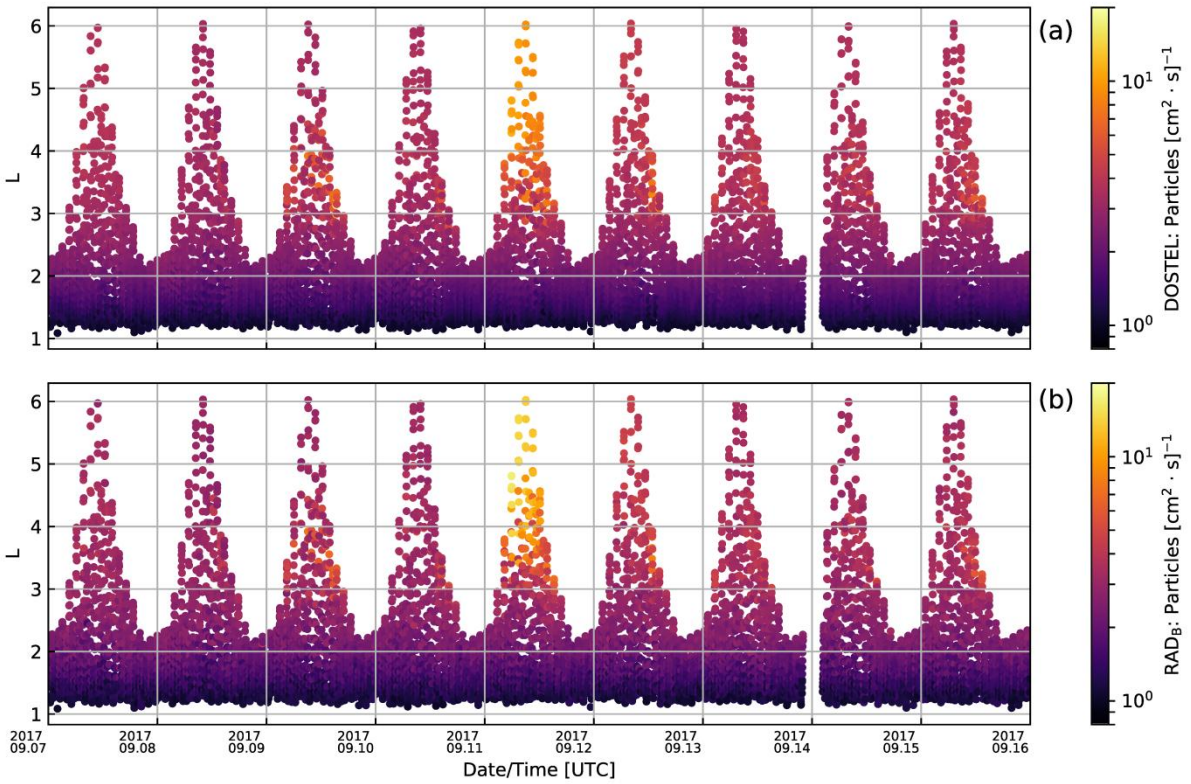

Figure 6. Count rates as a function of time and L for (a) the DOSTEL-2 instrument and (b) the ISS-RAD_B sub-detector between the 7 and 16 of September, 2017. Note: Measurements are required to be simultaneously active for both instruments; the gap in near the 14 September is an artifact of ISS-RAD being commanded to a checkout mode for a downlink of bulk data.

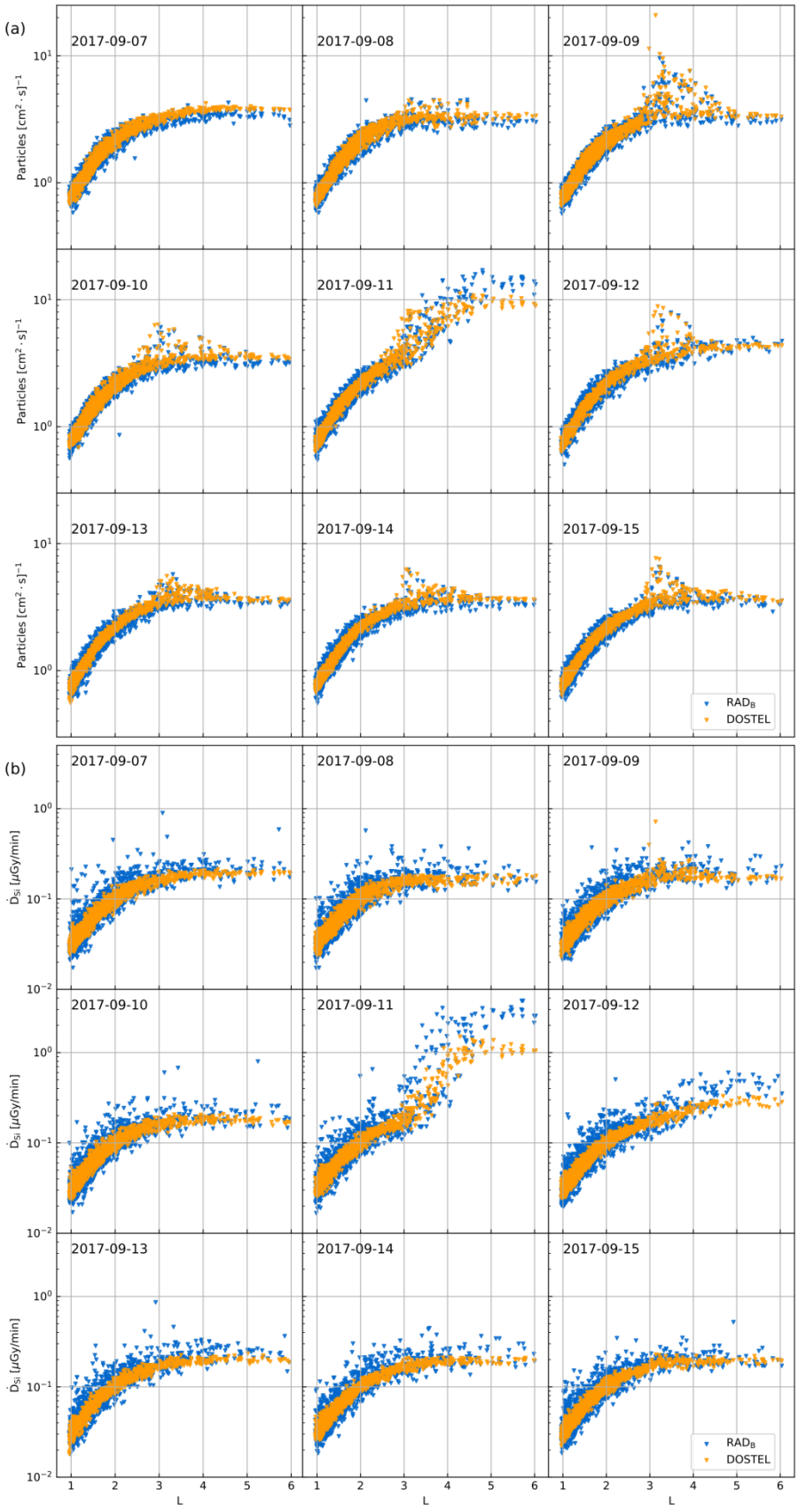

Figure 7. (a) Count- and (b) absorbed dose rates in Si for the DOSTEL-2 instrument and ISS-RAD_B sub-detector for each day from 7 to 16 September 2017. Note: SAA-like contributions have been cut out based on the procedure given at the start of Section 3

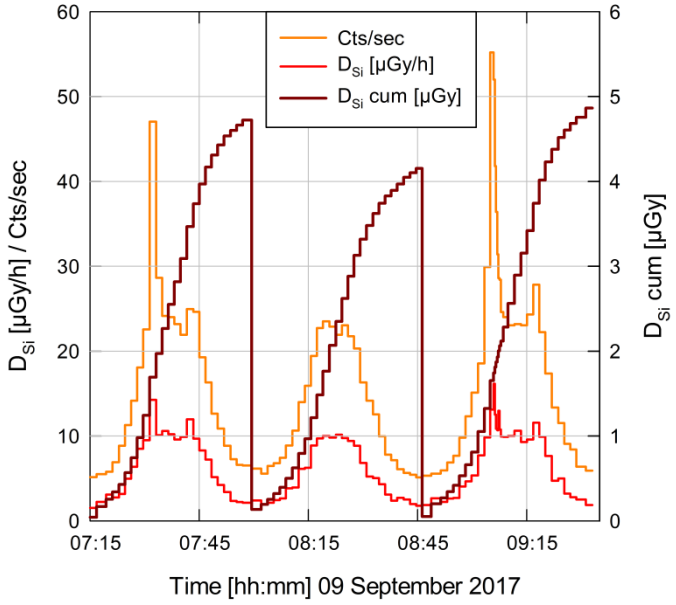

Figure 8. Count rate, absorbed dose rate in Si and cumulative absorbed dose for three consecutive half orbits of the ISS on the 9 September 2017 from 07:15 to 09:30 (UTC). The first and the third orbit are southern orbits, while the second one is a northern orbit.

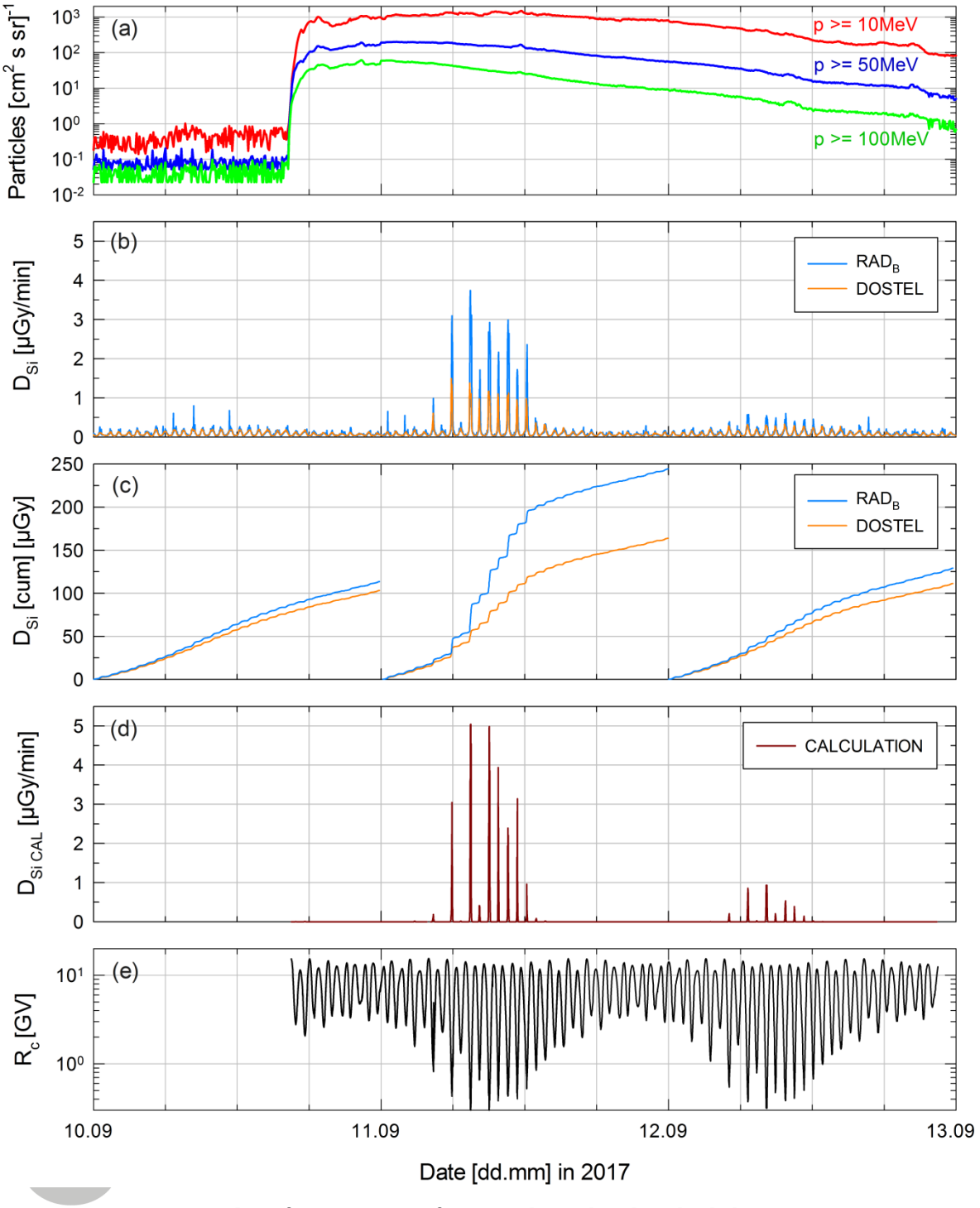

Figure 9. (a) GOES data for 10 to 13 of September; (b) absorbed dose rate in Si measured with the DOSTEL-2 instrument and the ISS-RAD$_B$ sub-detector for this time period; (c) cumulative absorbed dose in Si for each of the three days; (d) results of the DLR calculations and (e) respective R_C for the time of the event.

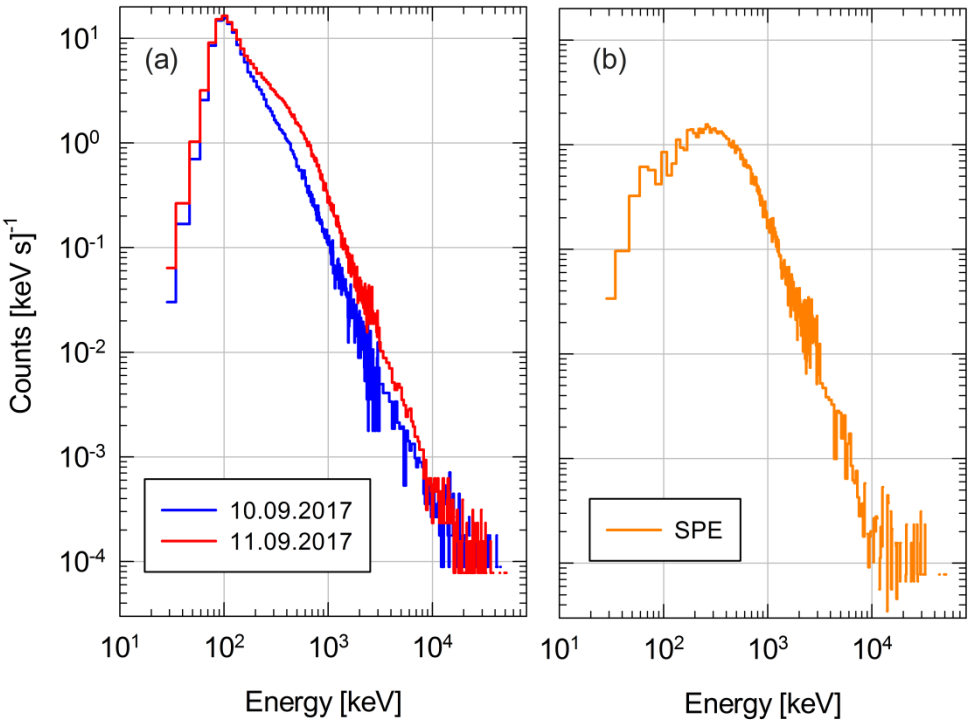

Figure 10. (a) Energy deposition spectra recorded with the DOSTEL-2 instrument for the day before the event and the day of the event; (b) SPE event spectra from the subtraction.

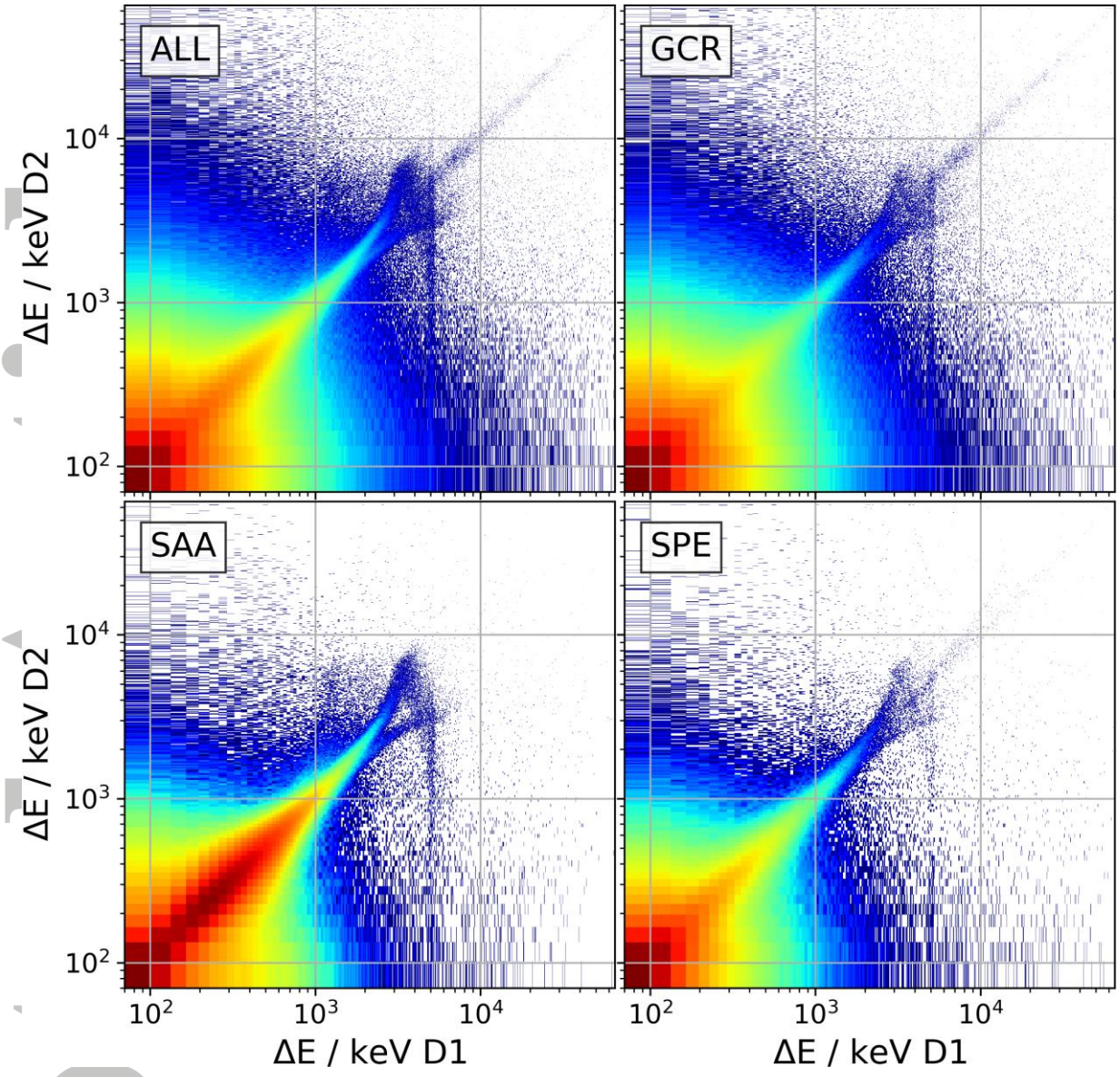

Figure 11. DOSTEL-1 instrument in Single Event Mode showing in (ALL) all energy depositions; (GCR) only GCR related energy depositions; (SAA) only SAA related energy depositions; (SPE) only energy depositions for the SPE.

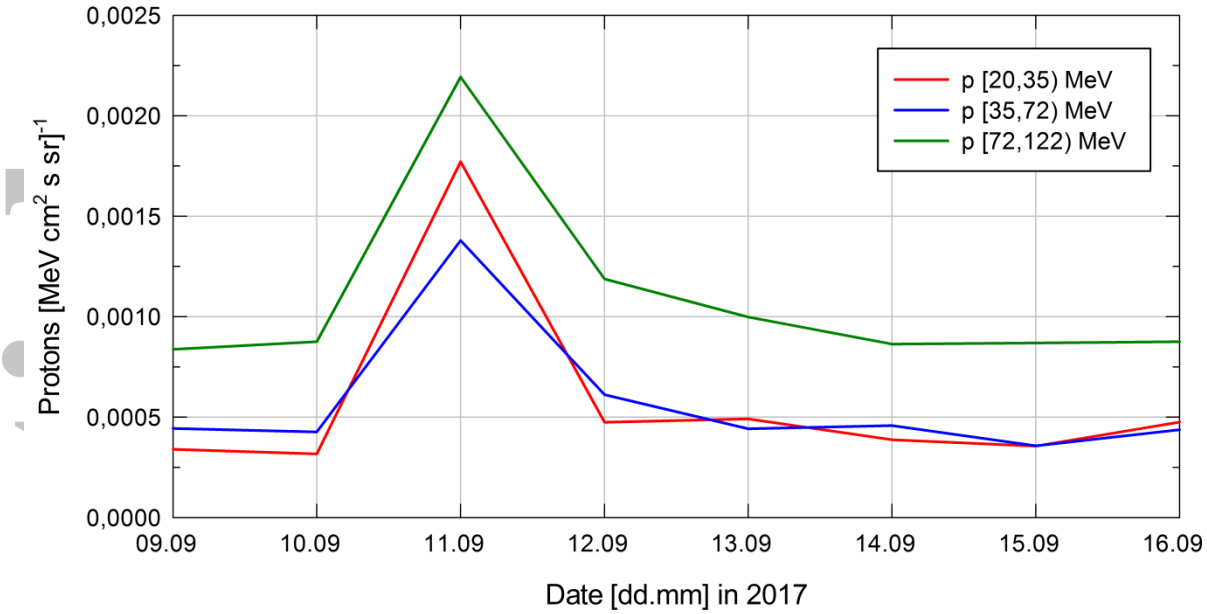

Figure 12. Proton flux from ISS-RAD$_D$ sub-detector for the three proton channels (20 – 35; 35 – 72; and 72 – 122 MeV) for 9 to 16 of September 2017. NOTE: SAA-like contributions have been cut out based on the procedure described in the beginning of Section 3; also note that the data are selected for values of L > 3 in order to account only for SPE-like contributions.